N-doped Graphene Supported on N-rGO Nanosheets as Metal-free Oxygen Reduction Reaction Electrocatalysts for Zn-air Batteries

Ruili Song, [‡a] Xiaoting Cao, [‡a] Xiaoshuang Zhou, [b] Ningyi Yuan, [,a]

a.   Jiangsu Province Cultivation Base for State Key Laboratory of Photovoltaic Science and Technology, School of Materials Science& Engineering, Changzhou University, Changzhou 213164, P. R. China.

b.   Institute of Intelligent Flexible Mechatronics, Jiangsu University, Zhenjiang, 212013, China. E-mail: dingjn@ujs.edu.cn

Electrochemical Measurements:

All electrochemical tests were performed at 25℃ using an electrochemical workstation (CHI760E, CH Instruments, Inc., Austin, USA) connected to a rotating disk electrode device (RDE, AFMSRCE) made by Pine Instrument Company, which used a three-electrode system: a glassy carbon electrode (GC, Φ5 mm) supported catalysts as the working electrode, Hg/HgO as the reference electrode, and a graphite rod (Φ4 mm) as the counter electrode. The glass-carbon ring disk electrode (the disk area is 0.2465cm^2, the ring area is 0.1886 cm^2, and the collection rate is 37%) was used to explore the number of transferred electrons of catalysts and the yield of H_2O_2. In this study, all potential tests were converted to the potential of the standard reversible hydrogen electrode (RHE), which were calculated according to the Nernst equation: E(*vs*. RHE)=E(*vs.* Hg/HgO) +0.098+0.059PH. The glassy carbon electrode was needed to be polished on the suede with a 0.05 μm Al_2O_3 polishing solution, and then the electrode was ultrasonically cleaned with deionized water.

The synthesis of catalyst ink: 5.0 mg of catalyst was dispersed in ethanol, water and 5 wt% Nafion mixture (Sigma-Aldrich) ($V_{ethanol}$:V_{water}:V_{Nafion}=800μL:190μL:10μL) to prepare catalyst ink. The solution was sonicated for at least 60 min to obtain a uniform suspension. Then, 14 μL of catalyst ink was drop onto the glassy carbon working electrode. The solution was sonicated in an ice bath for at least 60 min to obtain a uniform suspension. The loadings of both the catalysts prepared in this work and 20 wt% Pt/C on the working electrode were 0.35 mg cm^{-2}.

In order to evaluate the electrochemical performance of the catalyst, CV and LSV tests were performed in 0.1 M KOH electrolyte. Before all electrochemical tests, N_2 or O_2 was introduced for at least 30 min to ensure that the electrolyte contains saturated N_2 or O_2 during the test. O_2 was always introduced to ensure that the O_2 is saturated in the electrolyte during the LSV testing. The LSV test was performed at a scan rate of 10 mV/s, and the rotating speed of the disk electrode was 1600 rpm, and the potential range was 0.2V-1.1 V *vs*. RHE.

The LSV curve tests were performed at different speeds at 10 mV/s. The speed range of the rotating disk electrode was from 400 to 2500 rpm (400 rpm, 625 rpm, 900 rpm, 1225 rpm, 1600 rpm, 2025 rpm, 2500) rpm), the

electron transfer number (n) can be calculated according to the Koutecky-Levich (K-L) equation:

$$\frac{1}{j} = \frac{1}{j_K} + \frac{1}{j_{lim}} = \frac{1}{j_K} + \frac{1}{B\omega^{1/2}}$$

$$B = 0.62nFC_0D_0^{2/3}\upsilon^{-1/6}$$

Where j is the measured current density, j_K and j_{lim} are the kinetic and diffusion limit current density, ω is the angular velocity of the disk electrode, n is the number of electrons transferred, F is the Faraday constant (96485 C mol^{-1}), D_0 is O_2 Diffusion coefficient (the value is $1.9 \times 10\text{-}5$ cm^2 s^{-1} in 0.1 M KOH), C_0 is the volume concentration of O_2 ($1.2 \times 10\text{-}6$ mol cm^{-3}), and υ is the kinematic viscosity of the electrolyte (0.01 cm^2 s^{-1}).

For RRDE test, the test potential range of the disk electrode was 0.2V-1.1 V *vs*. RHE, and the scanning speed was 10 mV s^{-1}. The test potential of the ring electrode was 1.48 V *vs*. RHE. The number of transferred electrons (n) and the yield rate of H_2O_2% were calculated by the following formula:

$$n = \frac{4j_D}{j_D + \dfrac{j_R}{N}}$$

$$H2O2\% = 200\% \times \frac{\dfrac{2j_R}{N}}{|j_D| + \dfrac{j_R}{N}}$$

Where j_D is the disk current, j_R is the ring disk current, and N=0.37 is the Pt ring current collection rate.

Zn-air battery test: The Zn-air battery test was performed by a self-made device. The air cathode was composed of four layers, including: waterproof membrane, current collector foamed nickel, and catalyst on the surface of hydrophilic carbon paper. The catalyst side was in contact with the electrolyte. A mixed solution of 0.2 M Zn(Ac)$_2$ and 6 M KOH was used as the electrolyte. The polished 0.3 mm zinc plate serves as the anode. The effective area of the gas diffusion layer was 1 cm^{-2}, and the supported catalyst was 2 mg cm^{-2}. The discharge polarization curve of the zinc-air battery was tested at 5 mV s^{-1} by the electrochemical workstation. The galvanostatic discharge durability performance of Zn-air battery was tested at 10 mA cm^{-2} by the electrochemical workstation. According to the discharge curve, the corresponding specific capacity (mA h gZn^{-1}) and energy density (W h kgZn^{-1}) can be calculated by the following formulas:

$$Specific\ capacity = \frac{current \times service\ hours}{weight\ of\ consumed\ Zn}$$

$$Energy\ density = \frac{current \times service\ hours \times average\ discharge\ voltage}{weight\ of\ consumed\ Zn}$$

Characterization Methods: The crystal structure of the samples was determined by X-ray powder diffractometer (XRD) (D8 ADVANCE model of Bruker, Cu Kα radiation, λ = 1.5406 Å). The microstructure of the samples was obtained by field-emission scanning electron microscope (FESEM, SU8020) and high-resolution transmission electron microscope (HRTEM, Tecnai G2 F20 S-TWIN). The chemical state and element composition of the samples were recorded by using an X-ray photoelectron spectrometer (XPS, Thermo ESCALAB 250Xi, test parameters of single-color Al Ka (hv =1486.6 eV), power: 150 W; beam spot: 500 μm), using the Gauss-Lorentz function in the Advantage software and nonlinear smart background fit, all the XPS spectra were analyzed. The thermogravimetric analysis (TGA) curves were obtained by the NETZSCH (TG 209 F3) thermogravimetric analyzer, and the heating rate is 10℃ min^{-1} to 900℃ in N$_2$ atmosphere. The FT-IR was measured by the Fourier Transform Infrared Spectrometer of Thermo Fisher in the United States. The specific surface area and pore size of the samples were measured on a physical adsorption device produced by ASAP 2460 MAC Inc. The Raman spectrum was tested by a Raman spectrometer (Thermo scientific DXR Raman Microscope; excitation wavelength: 532nm). Element quantitative analysis was tested by the inductively coupled plasma (ICP-OES/MS, PE Avio200).
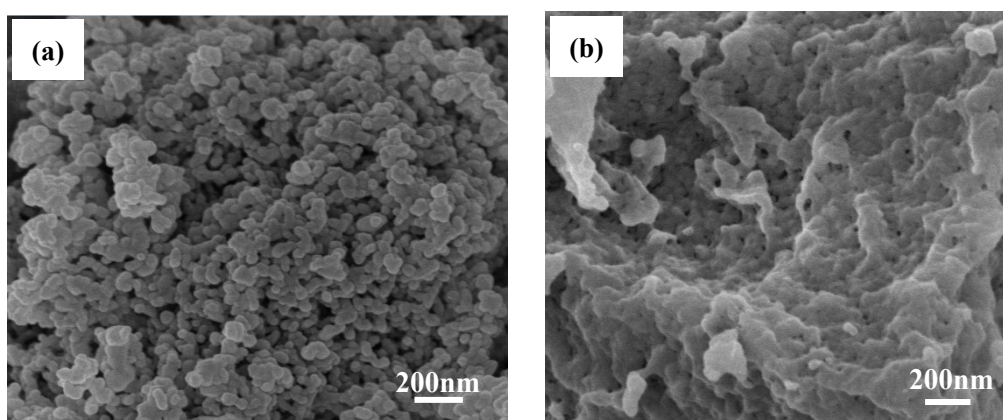

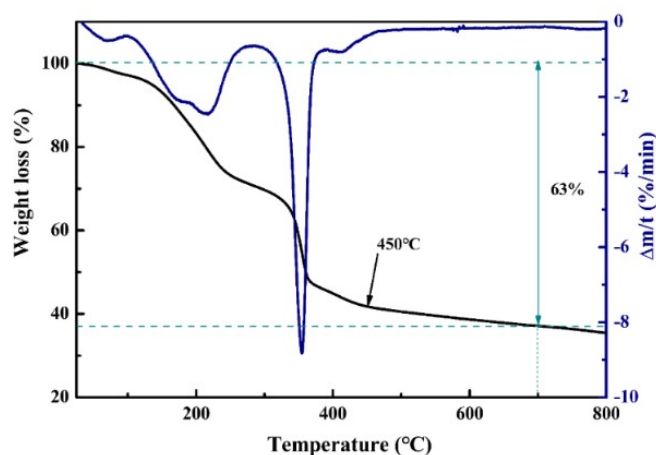Figure S1. (a) FESEM image of the Cu-BTC composite. (b) FESEM image of the N-graphene composite.

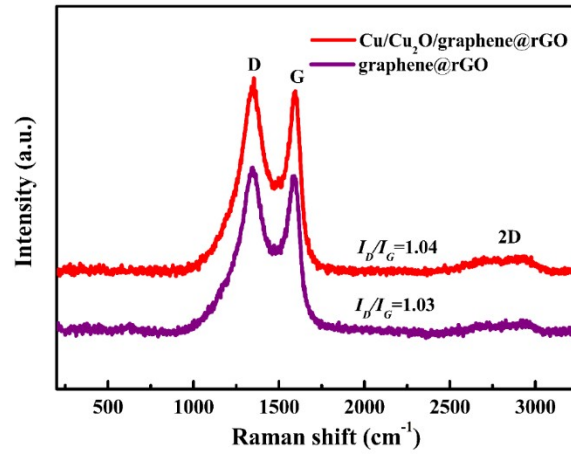Figure S2. TGA curve of Cu-BTC@GO precursor under nitrogen atmosphere.

Figure S3. Raman spectra of the Cu/Cu$_2$O/graphene@rGO and graphene@rGO composites.

Figure S4. (a) the N$_2$ absorption and desorption isotherm of the N-rGO composite. (Inset is the pore size distribution of N-rGO.) (b) the N$_2$ absorption and desorption isotherm of the Cu/Cu$_2$O/graphene@rGO composite. (Inset is the pore size distribution of Cu/Cu$_2$O/graphene@rGO.) (c) the N$_2$ absorption and desorption isotherm of the graphene@rGO composite. (Inset is the pore size distribution of graphene@rGO.) (d) the summary of the above N$_2$ absorption and desorption isotherms.
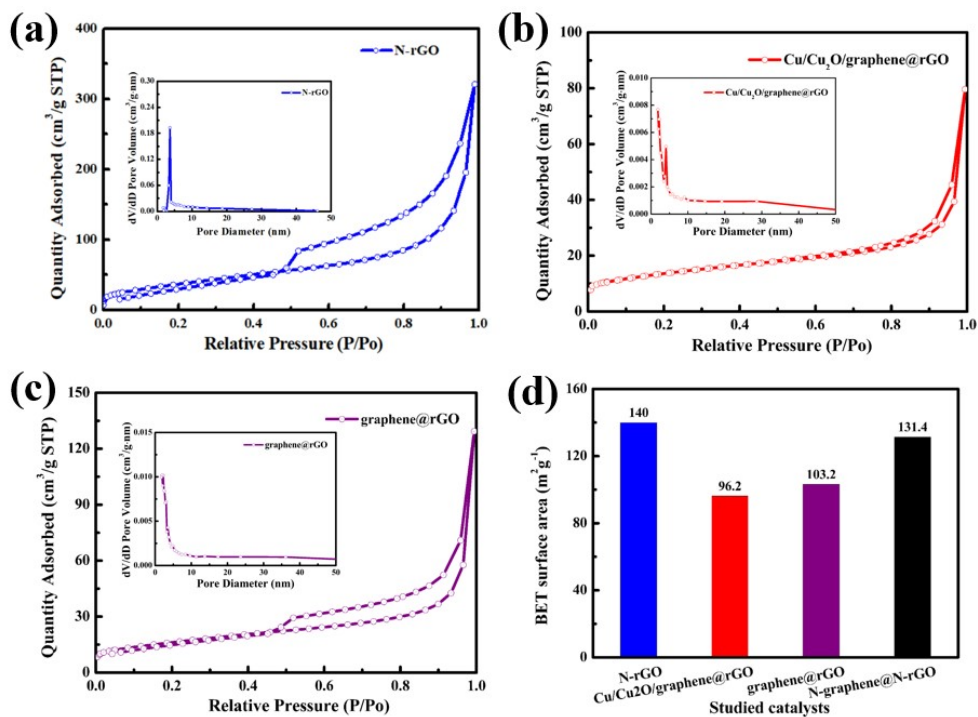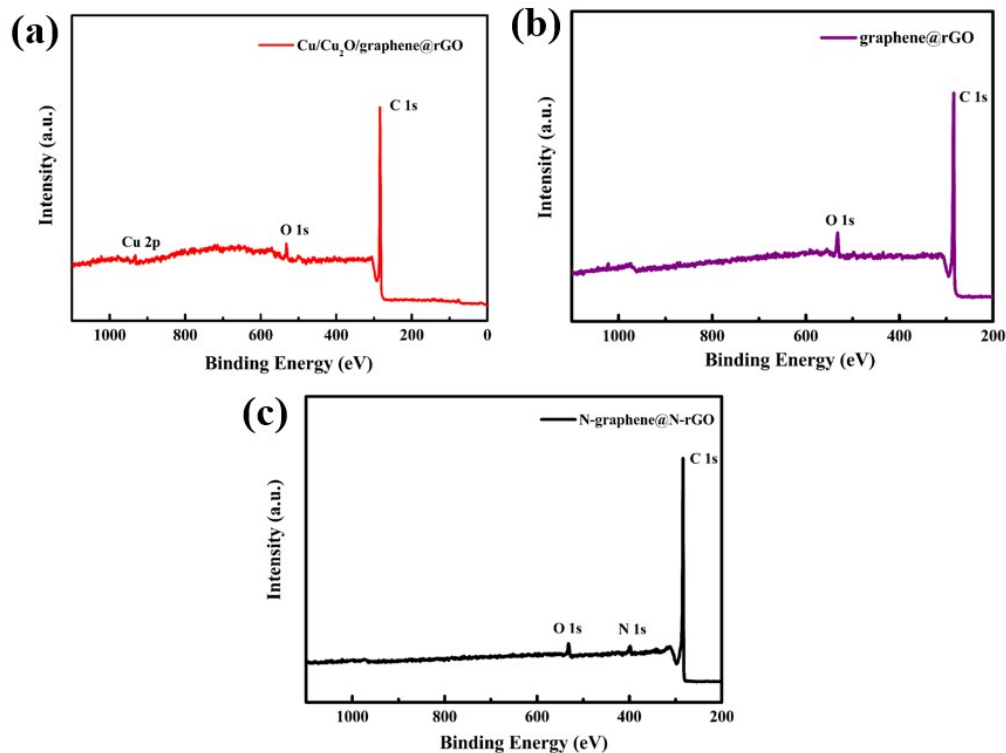
Figure S5. (a) the XPS survey of the Cu/Cu₂O/graphene@rGO composite. (b) the high-resolution Cu 1s XPS spectra of the Cu/Cu₂O/graphene@rGO composite. (c) the XPS survey of the graphene@rGO composite. (d) the XPS survey of the N-graphene@N-rGO composite.
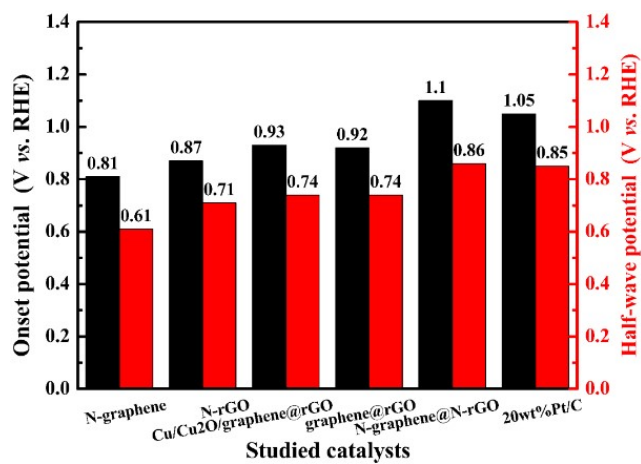

Figure S6. Onset potential and half-wave potential of N-graphene, N-rGO, Cu/Cu₂O/graphene@rGO, graphene@rGO, N-graphene@N-rGO, and 20 wt% Pt/C.
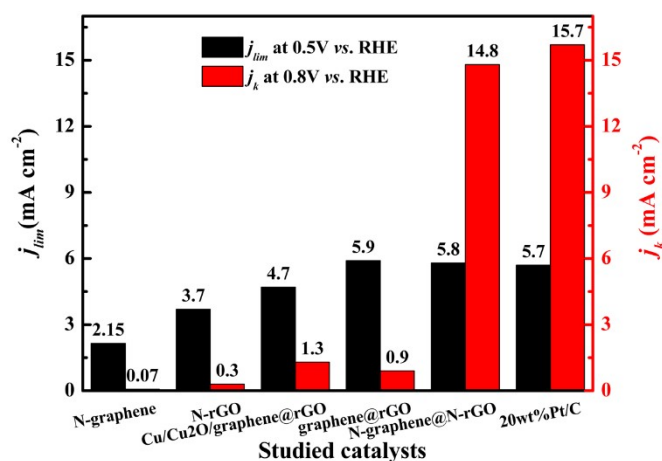
Figure S7. Kinetic current density at 0.8 V *vs*. RHE and limiting current density at 0.5 V *vs*. RHE of N-graphene, N-rGO, Cu/Cu$_2$O/graphene@rGO, graphene@rGO, N-graphene@N-rGO, and 20wt% Pt/C.
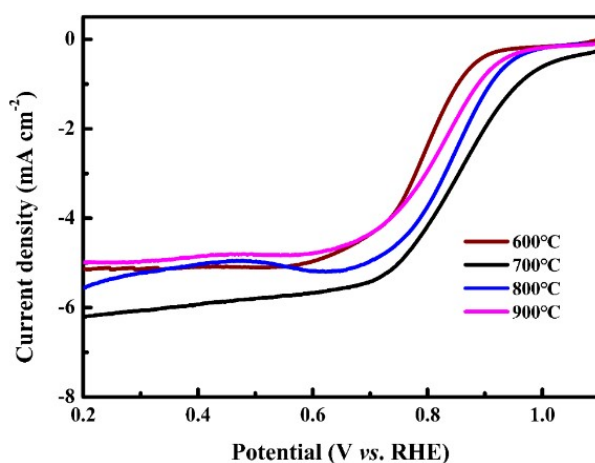

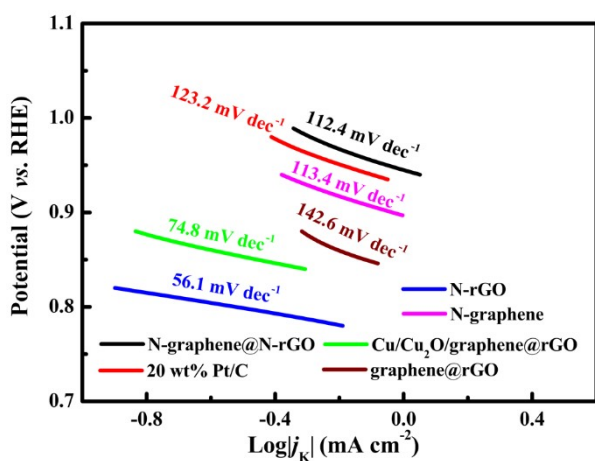Figure S8. LSV curves of N-graphene@N-rGO after different pyrolysis temperatures.

Figure S9. Tafel slopes of N-rGO, N-graphene, Cu/Cu$_2$O/graphene@rGO, graphene@rGO, N-graphene@N-rGO, and 20wt% Pt/C.
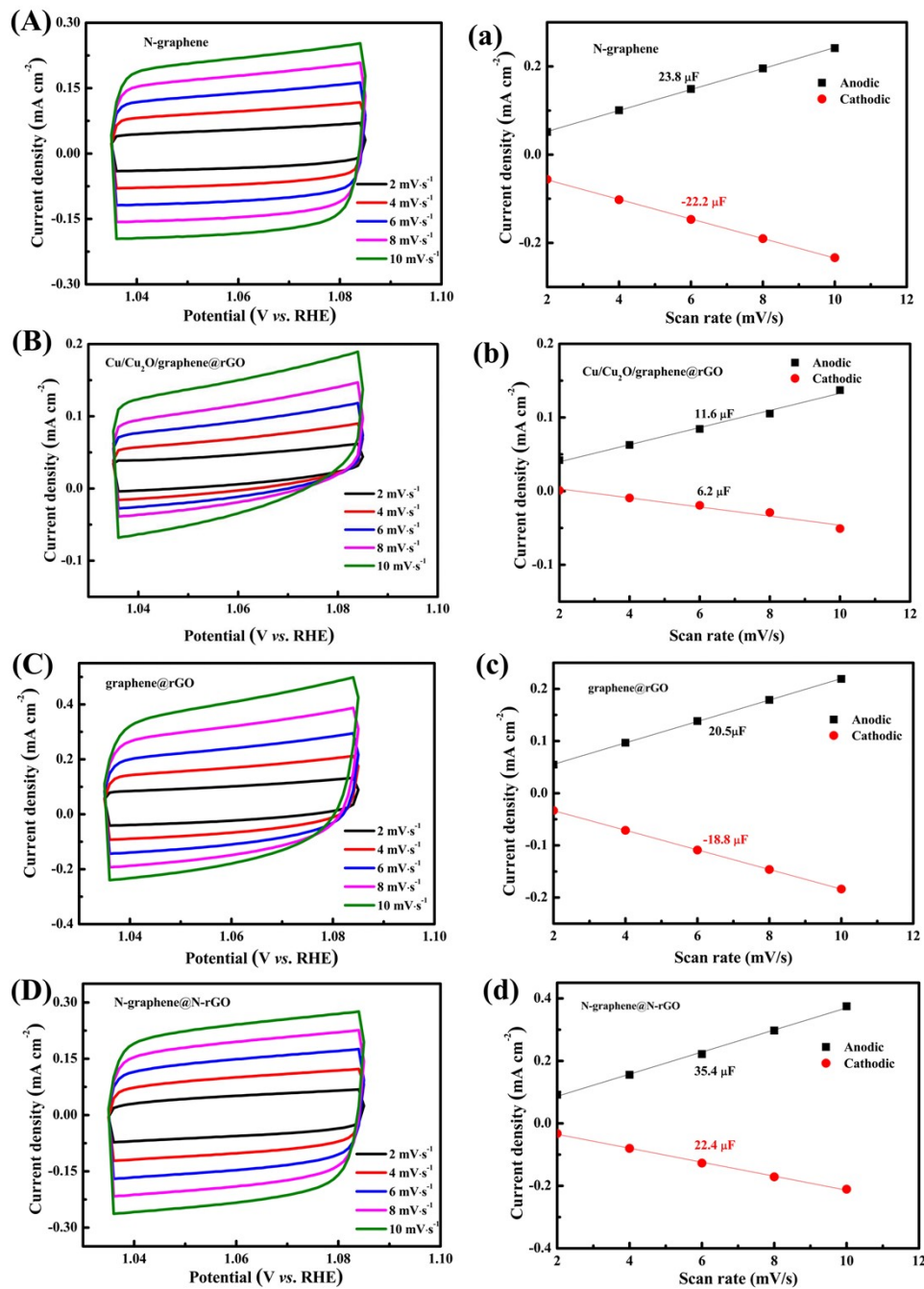
Figure S10. (A-D) CV curves measured at various sweep rates from 2 to 10 mV·s^{-1}, and (a-d) anodic and cathodic

plots of measured current at 1.05 V *vs*. RHE as a function of sweep rate for the samples.
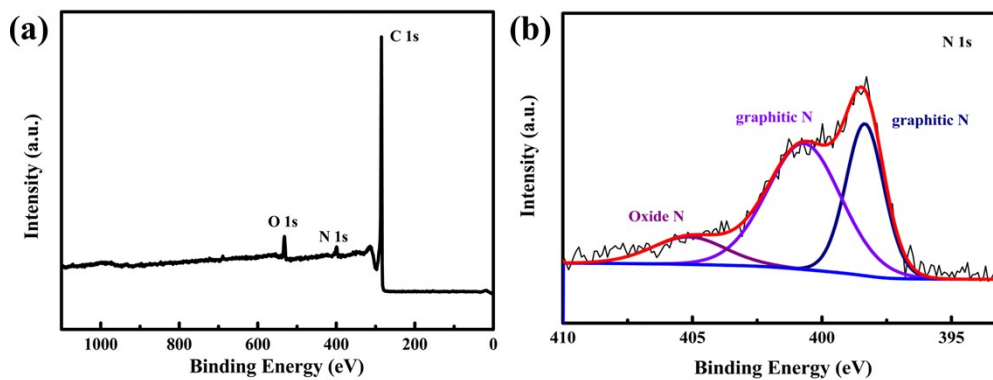
Figure S11. the XPS survey of N-graphene@N-rGO after the discharging stability test of Zn-air battery.

Table S1 ICP data of N-graphene@N-rGO

Sample quality, m_0 (g)	Constant volume, V_0 (mL)	Element	Solution for elemental concentration, C_0 (mg/L)	Element content, W (%)
0.0276	100	Cu	1.506	0.346%

Table S2 Comparison of electrocatalytic activities of N-graphene@N-rGO with the state-of-the-art metal-free catalysts

Sample name	Heteroatom	Loading (mg cm^{-2})	Half-wave potential (*vs*. RHE)	Limit current density (mA cm^{-2})	Reference
N-graphene@N-rGO	N	0.35	0.86	5.8	This work
HPNSC	N, S	0.25	0.87	-	1
P-G	P	-	0.77	-	2
ND-GLC	N	-	0.875	-	3
N,F-Carbon	N,F	-	0.84	5.2	4
NSC-A2	N,S	0.318	-	4.58	5
NPC	N	0.2	0.864	5.65	6
NG900	N	0.1	0.846	5.83	7
SNG	S, N	0.128	0.72	-	8
N,P-MC	N,P	0.2	0.84	5	9
mesoCF	N	0.25	0.87	-	10

References

(1) Y. Cheng, Y. Wang, Q. Wang, Z. Liao, N. Zhang, Y. Guo, Z. Xiang, *Journal of Materials Chemistry A*, 2019, *7*(16), 9831-9836.

(2) L. Tao, Q. Wang, S. Dou, Z. Ma, J. Huo, S. Wang, L. Dai, *Chem. Commun.*, 2016,**13**(52), 2764-2767.

(3) J. Zhang, Y. Sun, J. Zhu, Z. Kou, P. Hu, L. Liu, S. Li, S. Mu, Y. Huang, *Nano Energy*, 2018, **52**, 307-314.

(4) Y. Lv, L. Yang, D. Cao, *ACS applied materials & interfaces*, 2017, **9**(38), 32859-32867.

(5) S. Yang, X. Mao, Z. Cao, Y. Yin, Z. Wang, M. Shi, H. Dong, *Applied Surface Science*, 2017, **427**, 626-634.

(6) H. Han, Y. Noh, Y. Kim, W. S. Jung, S. Park, W. B. Kim, *Nanoscale*, 2019, **11**(5), 2423-2433.

(7) Y. She, J. Chen, C. Zhang, Z. Lu, M. Ni, P. H. L. Sit, M. K. Leung, *Applied Energy*, 2018, **225**, 513-521.

(8) F. Liu, F. Niu, T. Chen, J. Han, Z. Liu, W. Yang, Y. Xu, J. Liu, *Carbon*, 2018, **134**, 316-325.

(9) Z. Zhang, J. Sun, M. Dou, J. Ji, F. Wang, *ACS applied materials & interfaces*, 2017, **9**(19), 16236-16242.

(0) J. Gao, Y. Wang, H. Wu, X. Liu, L. Wang, Q. Yu, A. Li, H. Wan, C. Song, Z. Gao, M. Zhang, N. Ma, J. Wang, W. Zhou, G. Wang, Z. Yin, D. Ma, *Angewandte Chemie.*, 2019, **131**(42), 15233-15241.